Debris Characterization, Albedo, and Plume Measurements from Laser Ablations of Satellite Materials in High-Vacuum and in Gaseous Ambients

Gouri Radhakrishnan
Paul M. Adams
Diana R. Alaan
Christopher J. Panetta
Space Materials Laboratory, The Aerospace Corporation
Mail Station M2-248, 2310 E. El Segundo Blvd., El Segundo, CA 90245

ABSTRACT

The albedo of orbital debris fragments is a critical parameter in the derivation of their physical sizes from optical measurements. A variety of processes can alter the optical surface characteristics of orbital debris fragments in low earth orbit, resulting in a change in their albedo. The critical processes include scattering due to micron and sub-micron particles on the surface, effects of atomic oxygen, and space radiation effects (weathering). Here we mainly focus on the formation and effects of micron and submicron particles, generated during hypervelocity collisions. While field testing of hypervelocity impact (HVI) has been conducted, there are no known hypervelocity collision ground tests that simulate the high-vacuum conditions of 10^{-8} Torr or less that exist in the Low Earth Orbit (LEO) environment. Pulsed laser ablation in high vacuum offers an inexpensive laboratory simulation of hypervelocity impact under low-earth orbit like conditions and allows for well-controlled investigations that can be coupled to optical albedo (reflectance) measurements. We have previously demonstrated that laser ablations in low-pressure air offer many similarities to the recent DebrisLV and DebriSat hypervelocity impact experiments, while ablations in high-vacuum provide critical distinctions.

The results on the laser ablation of some of the representative target materials used in current satellite structures, such as 6061 Al alloy, stainless steel, and carbon composite are presented. Debris generated is optically characterized with UV-VIS-NIR reflectance, and corresponding particle size distributions are measured. Additionally, the ablated plume is characterized in-situ with time-resolved spectroscopic diagnostics in the sub-microsecond time regime identifying atoms and ions in the plume, allowing a correlation of the energetics of the ablated plume with resulting albedo and particle size distributions of ablated debris. In addition, comparisons are made between plumes and debris generated from 6061 Al in high-vacuum and in controlled gaseous ambients, such as air, oxygen, and nitrogen that reveal the roles of plume chemistry and collisional cooling. We have specifically addressed the issue of “debris darkening” and its root cause. We have attempted to recreate darkening by extending our investigations from metal targets to a composite target, and combining the effects of composite ablation on the surface of ablated 6061 Al. These results have relevant implications for the determination of physical sizes of orbital debris in LEO or Geosynchronous Orbit (GEO) that are based upon optical measurements that use albedo as a critical parameter.

1. INTRODUCTION

Understanding space debris relies heavily on an understanding of hypervelocity impact (HVI), which in turn plays a crucial role in current fragmentation modelling predictions. Low earth orbit (LEO) and geosynchronous orbit (GEO) are the most crowded orbits and numerous radar and optical measurements are being conducted to identify the material composition of space debris, as well asestablish their physical sizes [1-9]. The major concern with debris is that it might hit an operational spacecraft or a larger manned object such as the International Space Station (ISS) with detrimental consequences. Hence there is a basic need to gather orbital object data to accurately define the space environment for detection and trackingof debris object sizes [1-10] for space situation awareness (SSA), for which albedo of debris surfaces is critical.

A critical parameter for the interpretation of physical sizes of the space debris particles from optical measurements is the albedo of the fragments [4-6]. Currently observations of debris for SSA in LEO are conducted with radar [1-3], while optical observations are mostly used for observation of debris in GEO [7-10]. In 2007, National Aeronautics and Space Agency, Johnson Space Center recommended the use of a mean global albedo value of 0.13 for debris objects [4], then revised this to 0.175 [5]. As called out by the authors, additional calculations from alternate photometric data and research are needed for establishing more accurate albedo values (for more accurate size estimation). Since these albedo numbers are so critical to the determination of physical size of orbital debris, laboratory experimental measurements of albedo are relevant.

In order to get a true representation of HVI in low-earth orbit (LEO), ground-based experiments simulating the impact have to be conducted at extremely low pressures of 10^{-8} Torr or lower, that are representative of the LEO environment. A gun range can offer a realistic representation of the energy of impact and fragmentation, however, the background pressure that is available for practical reasons is limited to about 2 Torr.

According to Pirri [11], the use of laser ablation to simulate hypervelocity shock in a material could be accomplished by setting the laser spot equal to the diameter of the particles and the pulse duration equal to the particle impact duration.

Laser ablation differs from hypervelocity impact in that the laser material interaction occurs at the surface, leading to rapid heating and vaporization of the surface layer. This then results in a high pressure that creates a shock in the target. In hypervelocity impact, the projectile goes right through the bulk of the target, resulting in extensive fragmentation, with localized melting and vaporization, and ionization (plasma). It is the vaporization and melting associated with HVI that laser ablation simulates.

Laser ablation experiments can be conducted in high-vacuum (10^{-7}-10^{-8} Torr) and offer the flexibility of selecting any gaseous ambient, at any controlled pressure, thus allowing for comparison to the hypervelocity impact experiments in low-pressure air. Another important attribute of conducting laboratory measurements is that it does not require foam catch panels (used in DebrisLV and DebriSat experiments [12,13] to catch fragments) that interfered with microscopic debris analyses and albedo measurements. Experiments are coupled with optical characterizations (UV-VIS-NIR reflectance), chemical characterization, surface morphology, and particle size distributions of the debris. We demonstrated our ability to duplicate DebriSat hypervelocity gun-range test data [12,13] in 2 Torr of air using the laser ablation technique and used this as a baseline for recreating the deposition process that occurs during hypervelocity collisions in high-vacuum [14,15]. We showed that the albedo of debris fragments is dependent on the optical properties of surface coatings comprising nano-micro particulates generated by impact [15].

In this work, we have extended the laser ablation of 6061 Al to additional spacecraft materials such as stainless steel and carbon composite. The rationale for doing these materials is to address the question that poses the greatest interest, namely, “debris darkening” and its root cause. Both the space environment and hypervelocity impact could result in the “darkening” i.e. decrease in optical reflectance or albedo of orbital debris. As stated before, these changes in albedo in turn are being used as inputs to the calculation of the physical sizes of debris objects [4-6].

Likely mechanisms for hypervelocity impact related debris darkening could be the formation of nanometer sized grains of metals, or the deposition of a highly absorbing material such as carbon. Previous laboratory hypervelocity impact studies have implicated the role of the breakdown of plastics in circuit boards in producing a thin soot layer that blackened surfaces [6]. In the DebriSat tests, very dark surfaces on fragments were attributed to coatings of disordered graphitic carbon, which were a byproduct of the hypervelocity impact plasma interacting with soft catch foam that lined the vacuum chamber [13]. While this was an artifact of the DebriSat tests, one might expect similar results from the interaction of organic materials (multilayer insulation, printed circuit boards, wire insulation) on spacecraft in a hypervelocity impact where vaporization and plasmas are produced. Here we have attempted to recreate hypervelocity impact darkening by extending our investigations from metal targets to a carbon-fiber-reinforced composite target, and combining the effects of composite ablation on the surface of ablated 6061 Al.

.

2. EXPERIMENTAL

Ablation targets included 6061 Al alloy, 316 stainless steel, and a carbon fiber composite. Pulsed Laser Ablation (PLD) was conducted in vacuum and in air with a high-power excimer laser (Lambda-Physik LPX 210i). The target (1” diameter disc), was held in a stainless-steel vacuum chamber at a 45-deg angle to the incoming laser beam. The chamber is pumped by a turbomolecular pump to a maximum base pressure of 10^{-8} Torr, and has gas inlets for various gases. Laser ablations of the 6061 Al target were conducted both in 2 Torr air, as well as in high vacuum (10^{-7} Torr), while the 316 stainless and composite target were only ablated in high vacuum.

Deposited materials were collected on single-crystal silicon, fused silica and polished 304 stainless steel (SS) substrates held at a distance of ~ 50 mm in front of, and parallel to, the target. Spectroscopic identification of atoms and ions in the ablation plume was conducted as a function of laser fluence. For comparisons with the gun-range HVI experiments we conducted [12,13] and as discussed previously [14,15], laser fluences of 7-9 J/cm^2 were employed for ablation. These measurements were made by imaging the plume through a fused silica port via a 3-m long optical fiber onto a gated ICCD camera, (PIMAX3) coupled to a spectrometer (320 PI). Following a TTL trigger input from the excimer laser supplied to the CCD camera, the CCD was gated with allowed gate widths ranging from 4 nanoseconds (ns) to 1 millisecond (ms). The spectrometer is equipped with 3 gratings: 150 grooves/mm and 600 grooves/mm, both blazed at 300 nm, and a holographic 2400 groove/mm grating blazed in the UV. Emission spectra shown here were taken at a distance of 1 mm from the target surface.

Deposited materials were examined in a JEOL 7600F field emission scanning electron microscope (FE-SEM) at 2KV to 15KV. Silicon samples were cleaved and the edges were examined to determine the thickness of deposits. Energy dispersive spectroscopy (EDS) was performed with an Oxford Instruments X-Max silicon drift detector (SSD) at 5KV to 20KV in order to control the penetration depth.

The percent of the substrate surface covered by particles was determined from automated particle analysis in the scanning electron microscope (SEM). Polished 304SSsubstrates (high-Z) were selected to provide backscatter contrast between the Al particles (low-Z) and substrate. By adjusting the accelerating voltage (10-15 KV) in the SEM the Al particles could be discriminated from the thin continuous Al film in the backscattered electron images. Thresholds (brightness/contrast) of the SEM images were adjusted to define particles vs. film/substrate and the image analysis software (Oxford Instruments: Feature) counted and sized all the particles in the field of view (FOV). The percent coverage was determined from the total area of particles in the FOV. The thickness of thin films was calculated from the EDS data using Oxford Instruments Layer Probe software.

Pre-and post-deposition optical characterizations (UV-VIS-NIR reflectance) on Si, fused silica, and stainless steel 304 (SS 304) substrates were conducted to understand debris darkening as a function of impact conditions

Total hemispherical reflection measurements were made with a Perkin Elmer Lambda 900 spectrophotometer equipped with a Labsphere PELA 1000 integrating sphere attachment. The PELA 1000 can also measure selectively the diffuse component of reflection by allowing the specular beam to exit the sphere (and, therefore, not be collected by the detector). From this, specular reflectance can be calculated by subtracting the diffuse component of the reflectance from the total hemispherical reflectance. For this work, reflection measurements were made at an 8-deg angle of incidence, relative to a Spectralon reference material. An NBS 2019d white tile was also measured in the same configuration, to make the relative measurements absolute. This was accomplished by comparing the relative reflection measurement of the tile with the certified values and applying correction factors to ensure the two spectra overlay. These factors would then commute to the scans of the samples.

3. RESULTS AND DISCUSSION

Laser ablation of a 6061 Al target was conducted in high vacuum (10^{-7} Torr) and in 2 Torr of air and 2 Torr of N_2. Scanning electron microscope (SEM) images of ablated Al are shown in Fig. 1. In high vacuum, a thin metallic film of Al is deposited along with flattened molten Al particles (splats) (Fig. 1a). In contrast, ablation of 6061 Al in 2 Torr air produces fine filaments of Al_xO_y and small, spherical Al particles, as shown in Fig. 1b, which closely match those observed in hypervelocity impact debris measured with Debris-LV [13]. In 2 Torr of pure N_2 gas, spherical Al particles are deposited (Fig. 1c), but there is an absence of the fine filaments, which are attributed to the Al_xO_y deposited in air due to reaction with the oxygen present.

In high-vacuum, the ablated material in the gas phase and molten droplets of Al from the target, travel to the substrate without collisions. The liquid droplets flatten upon impacting the substrate, and are observed as splats. In 2 Torr air, collisional cooling of the ablated plume by background gas molecules results in solidification of the ejected liquid Al droplets, in-flight, as they travel to the substrate, evidenced by perfectly spherical particles that are covered by a sheath of oxide, as opposed to flattened splats of Al metal. In addition, fine filaments (Al_xO_y) are produced and the nanometer sizes of these filaments indicate that these are produced from gas-phase reactions between ablated Al and oxygen in the air molecules. The gaseous N_2 helps solidify the liquid Al droplets ejected from the target, without the formation of Al_xO_y filaments.

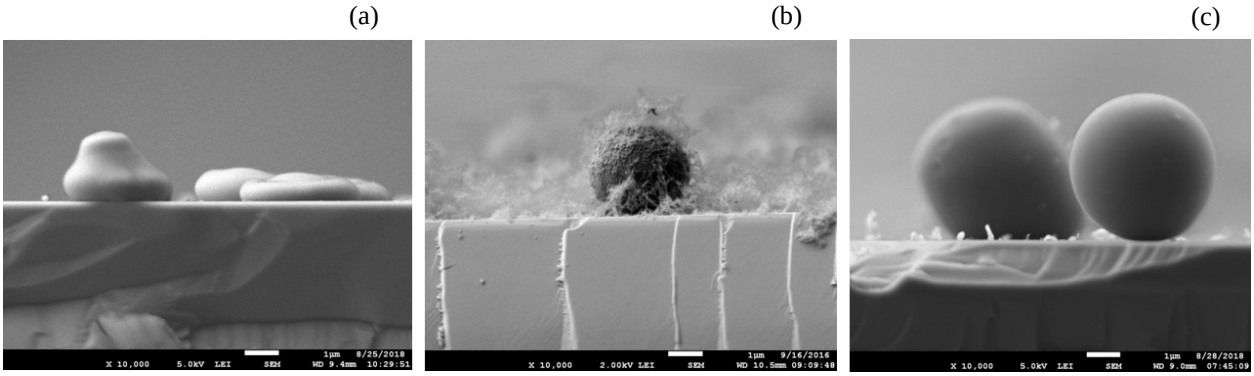

Fig. 1 SEM images of deposits on cleaved Si: 6061 Al ablation in high-vacuum showing flattened splats of Al (a), 6061 Al ablation in 2 Torr air showing filaments of Al_xO_y on a spherical Al particle (b) 6061 Al ablation in 2 Torr N_2 showing spherical particle of Al without Al_xO_y filaments

Laser ablation of a 6061 Al target at a vacuum of 10^{-7} to 10^{-8} Torr produces both neutral atomic Al (I) and singly charged Al (II) ions, as also seen in other work [16]. High-resolution spectra of the ablated plume were measured with a 2400 gr/mm grating. Atomic Al (I) with characteristic doublet peaks at 308.2 nm, 309.3 nm, 394.4 nm and 396.2 nm, and singly charged Al (II) with a peak at 466.3 nm [17] were observed. These emission peaks are shown below in Fig. 2a, measured with a gate width of 10 ns and a delay of 150 ns. The ratio of ions to neutrals is a function of laser fluence and this ratio increases with increasing fluence. Below 6 J/cm^2, singly ionized Al I were too low in intensity to be detected.

In the presence of air at pressures of 0.5 Torr and greater, atomic and singly ionized Al are still readily detected, however, distinct vibrational bands from molecular AlO are observed after a 5-μs delay [14,15,18]. Low-resolution AlO vibrational bands in 2 Torr air, measured with a 300 groove/mm grating are shown in Fig. 2b, measured with a gate width of 1μs. The vibrational transitions are from levels in the $B^2\Sigma$ - $X\ ^2\Sigma$ electronic transition [19] with a series of vibrational band sequences (Δv = 3, 2, 1, 0, -1). These AlO bands are absent in the high-vacuum ablation plume.

In 2 Torr nitrogen (N_2), no emission from the (0,0) band of the molecular AlN A $^3\Pi_i$- X $^3\Sigma_i$ system at 507.8 nm [19] is detected, although atomic and singly ionized Al are still detected. This was the case with all fluences ranging from 7 J/cm^2 – 20 J/cm^2. We also did not detect ionized N II emission lines, even at the high fluences (> 10 J/cm^2) although Al II was readily detected. In addition, raising the N_2 pressure to 70 Torr also did not produce emission from AlN.

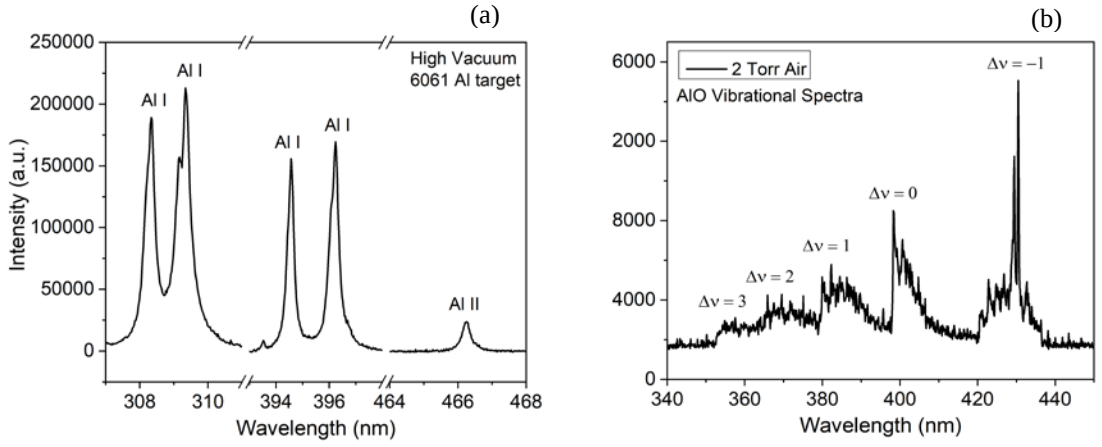

Fig. 2 Emission spectra of Al I and Al II lines in high vacuum (a); AlO vibrational bands in 2 Torr air (b)

In their study on the laser ablation of Al in 70 Pa (0.5 Torr) N_2, using a quadrupled Nd:YAG laser at 266 nm laser radiation, an energy of 15 mJ/pulse, and a fluence of 20 J / cm^2, Hermann and Dutouqnet [20] also reported that no emission from AlN was detected. However, Sharma and Thareja [21] reported the detection of AlN at 70 Torr N_2 pressure, with the fundamental mode of the Nd:YAG laser at 1064 nm, an energy per pulse of 300 mJ, and a spot size of 260 um, which would correspond to a fluence of 565 J/cm^2. These authors report the detection of N II emission lines, as well as Al II and Al III emissions. The fluence employed by these authors is nearly a factor of 30 greater than the highest fluence we attempted and a factor of 80 greater than the nominal fluence used. This could be the reason for the observed differences.

Optical reflectance measurements were made on the ablation deposits collected on fused silica substrates. Significant differences can be observed in the optical reflectance measured on ablated deposits produced in high-vacuum and in 2 Torr air, with ablations conducted at 7 J/cm^2 (Fig. 3).

In total reflectance (Fig. 3a), the reference uncoated fused silica substrate has a very low reflectance (< 4%), while the metallic Al film deposited in high-vacuum is highly reflective (60-80%). The transparent Al_xO_y film, deposited in 2 Torr air has a low reflectance similar to the fused silica substrate.

In transmission (Fig. 3b), fused silica is 90% transmitting over the entire wavelength range. Al_xO_y is also nearly 90% transparent, while Al has a transmission of < 5%.

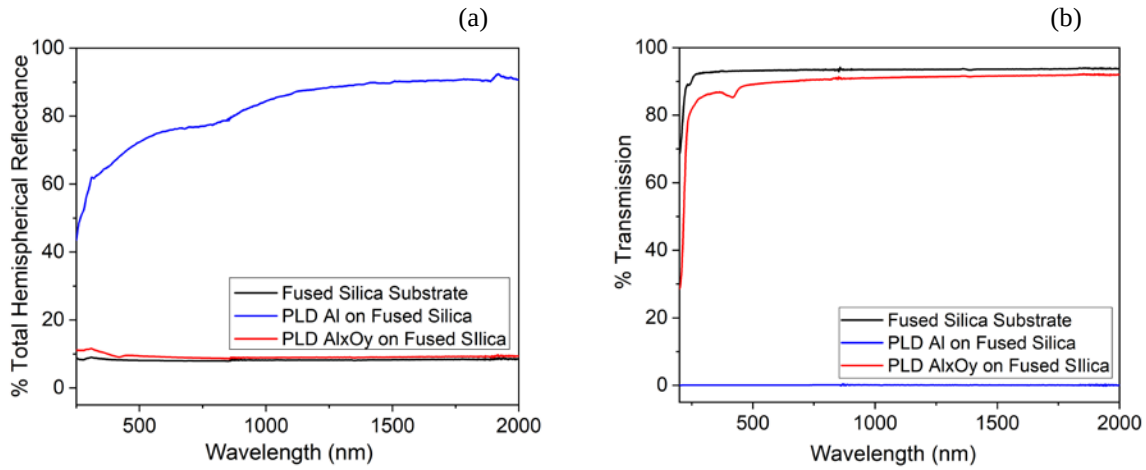

Fig. 3 Total hemispherical reflectance (a); transmission (b) of Al and Al_xO_y films formed in high vacuum and 2 Torr air, respectively

Laser ablation of 316 SS was also conducted in high vacuum. 316 SS is commonly used in spacecraft components, as part of frames, tubing etc. It has a material composition, by weight, of roughly 15 % Ni, 17% Cr,1-2% Mo, and nearly 66 % Fe. Fig. 4a shows the surface morphology of laser ablated 316 SS which produced a very thin (240 nm) smooth film and displays a low particle density (0.3% by area). Unlike the few lines present in the emission spectra of 6061 Al, the emission spectra of 316 SS are densely populated with numerous atomic emission lines from Fe, Cr, and Ni, and Fig. 4b shows one such spectral region dominated by Fe I lines, measured using a 600 groove/mm grating, gate width of 20 ns, and a gate delay of 150 ns.

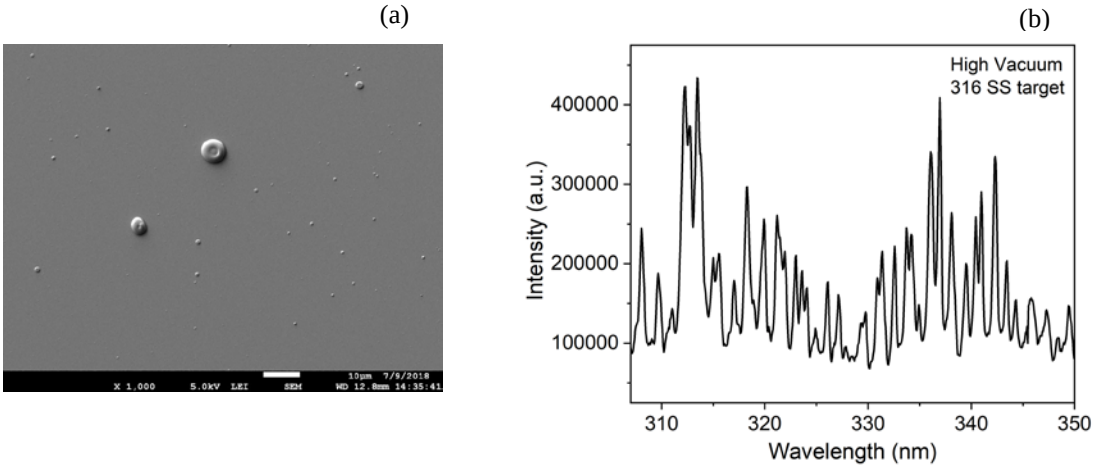

Fig. 4 SEM image of 316 SS film ablated in high vacuum on Si substrate (a); emission spectrum of ablated plume from 316 SS showing numerous Fe I spectral lines (b)

Shown in Fig. 5 are the optical reflectance spectra of 316 SS deposited on a Si (100) substrate. The total reflectance (Fig. 5a) ranges from 70% in the NIR to 40% in the UV. The contribution to the total reflectance of the smooth 316 SS film is almost entirely specular as indicated by the extremely low (< 1%) diffuse reflectance. The Si substrate is single-side polished and due to its absorption band edge at 1.1 eV, the Si becomes transparent at wavelengths greater than 1000 nm. Correspondingly, the diffuse and total reflectance spectra display a sharp increase > 1000 nm, which is due to scattering from the rough backside Si surface.

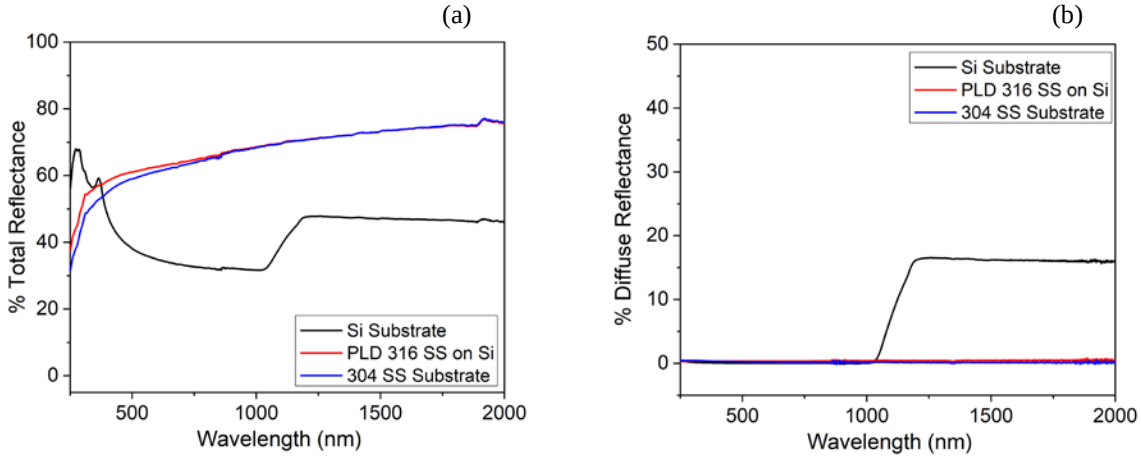

Fig. 5 Total hemispherical reflectance (a) and diffuse reflectance (b) of 316 SS film on Si; also shown in (a) are the reflectance of the Si substrate and a polished SS 304 substrate for comparison

We conducted studies to understand the correlation between the number of particles produced by laser ablation of a 6061 Al target as a function of incident laser fluence and how that affects reflectance. Three runs of laser ablation of the 6061 Al target were conducted in high vacuum (10^{-7} Torr) with the laser set at a repetition rate of 10 Hz and using approximately the same laser fluence (10.4 - 11 J/cm^2), with deposition times of 7.5 min, 15 min, and 30 min (Fig. 6). After each run, the percent coverage of the SS substrate with Al particulates and the average particulate size (equivalent circular diameter - ECD) was determined. Our results indicate that the percent coverage

by particles varies linearly with deposition time (Fig.7). Also, particulate ECD decreased from 1.96 µm to 0.96 µm as the particle coverage increased.

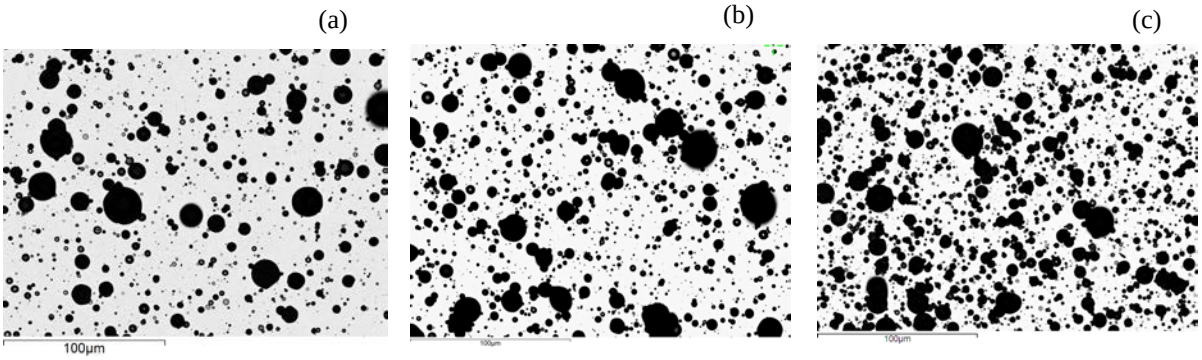

Fig. 6 Thresholded backscattered SEM images of PLD 6061 Al deposited on 304 SS substrates for 7.5 min (a), 15 min (b), and 30 min (c)

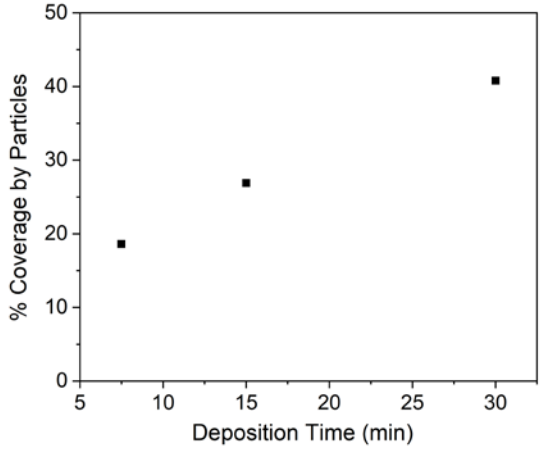

Fig. 7 Percent coverage of substrate surface by Al particles as a function of deposition time

Optical reflectance (total and diffuse) was measured following each deposition run. Equivalent optical measurements were also made on the reference SS substrates prior to deposition. Fig. 8 (a, b) shows the optical measurements. The total reflectance of all three 6061 Al films is around 90%, and much higher than the 304 SS substrate (Fig. 8a). However, the total reflectance decreases with increasing deposition time and is lowest for the film deposited for 30 min. This can be attributed to greater scattering losses from diffuse reflectance due to a higher particle density.

Fig. 8b shows a plot of the measured diffuse reflectance for the films deposited at 7.5 min, 15 min, and 30 min, and clearly shows that the diffuse reflectance increases with increasing deposition time. The dependence of diffuse reflectance with percent coverage is linear at short wavelengths (250 nm) and levels off slightly with increasing particle coverage (18.6% - 40.8%) at longer wavelengths (> 1 micron). The substrates are also covered with a thin continuous film of Al that increased in thickness from 99 nm to 218 nm as the deposition time increased. With increasing deposition time, the particle coverage increased correspondingly, hence the diffuse reflectance is seen to increase with increasing particle coverage (Fig. 9).

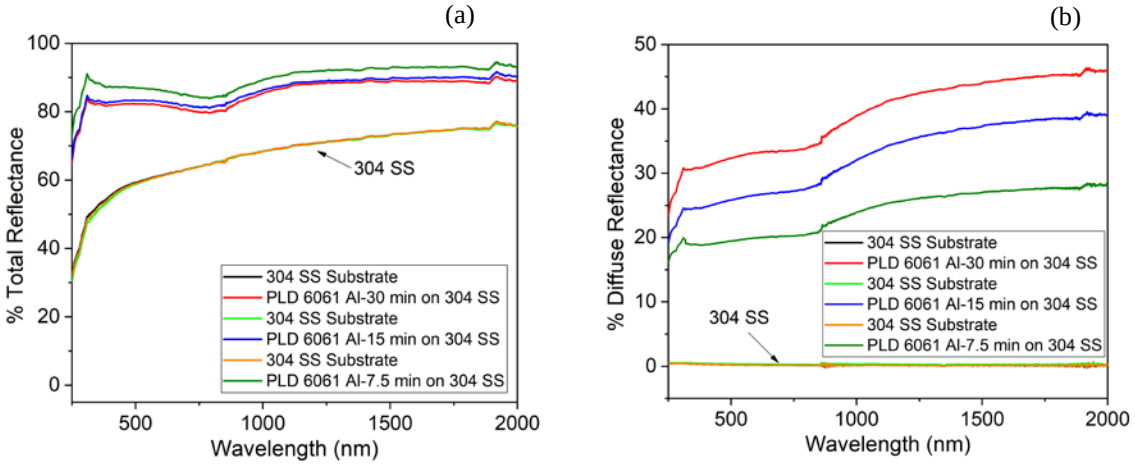

Fig. 8 Total reflectance (a) and diffuse reflectance (b) of 6061 Al films deposited on 304 SS substrates for 3 different deposition times of 7.5 min, 15 min, and 30 min; corresponding diffuse reflectance curves are shown in (b)

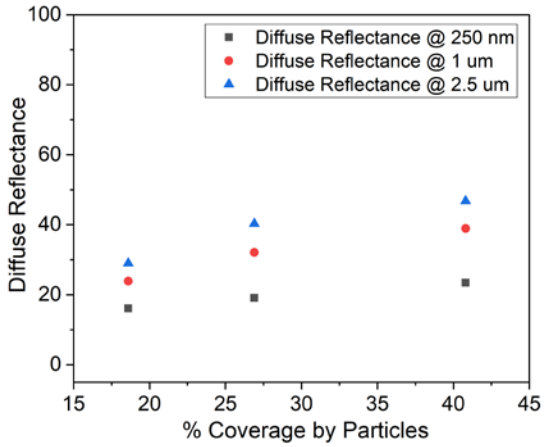

Fig. 9 Diffuse reflectance as a function of percent coverage by Al particles

These results can help get a rough estimate of particle coverage from optical reflectance measurements. Additionally, they can be a good indicator of how a hypervelocity impact changes the surface morphology by particle coverage and hence changes the optical characteristics of the debris surface.

Our results so far have shown that ablation of metal targets of typical spacecraft materials such as 6061 Al and 316 SS do not produce darkened surfaces. The reflectance can be lowered by scattering from particles on the surface of the metal, nonetheless, the reflectance is still high. To address the issue of “debris darkening” we proceeded to ablate a composite target that was PAN-based carbon fibers reinforced with a polysulfone-filled epoxy resin. Similar composites are commonly used as a facesheet on spacecraft 6061 Al honeycomb panels. We first attempted to ablate the composite, using Si as a substrate, however, it was not suitable for the deposition of carbon, and adhesion between the carbon and Si was very poor. Fig. 10 shows an SEM of the surface of the composite target before ablation (Fig. 10a) and the exposed carbon fibers following laser ablation of the surface (Fig. 10b). Fig. 10c shows a close-up of the ablated film from the composite target on a Si substrate.

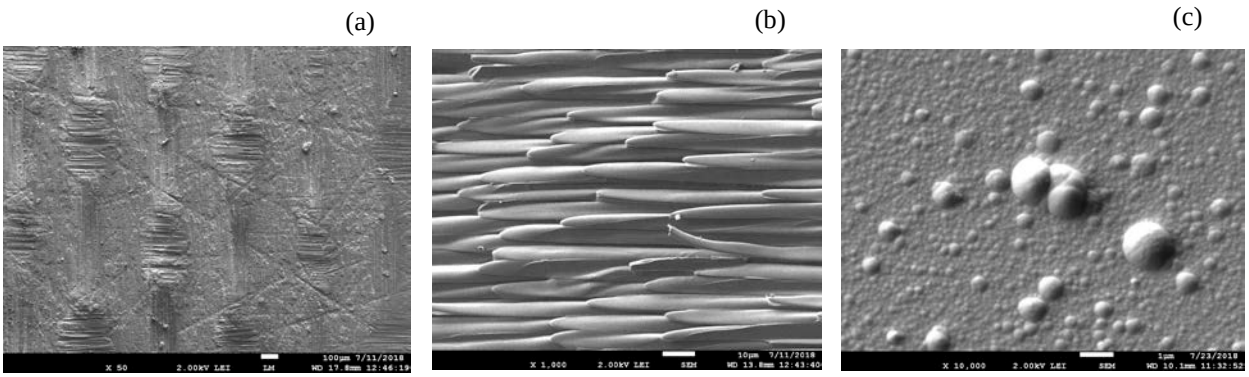

Fig. 10 SEM images of as-received carbon fiber composite (a); ablated surface of composite target showing carbon fibers (b); ablated composite film on a polished Si (100) substrate (c)

Fig. 11a shows a Raman spectrum of the composite film. The Raman spectrum indicates that the film is amorphous, as evidenced by a very broad peak centered at 1558 cm^{-1}, with a shoulder around 1300 cm^{-1}, instead of a distinct D band. The laser ablated plume shows very intense vibrational bands of the C_2 molecule which is characteristic of ablation from carbonaceous sources. Characteristic Swan band emissions from the C_2 molecule are observed and are shown in Fig. 11b. This spectrum was measured using a 300 groove/mm grating with a 100 ns gate and a delay of 750 ns. are due to vibrational transitions $\Delta v=1$, $\Delta v=0$, and $\Delta v=-1$ between the excited and ground electronic states $d\,^3\Pi_g \rightarrow a\,^3\Pi_u$, with band heads at 463.5 nm, 516.5 nm, and 550.5 nm [19] respectively.

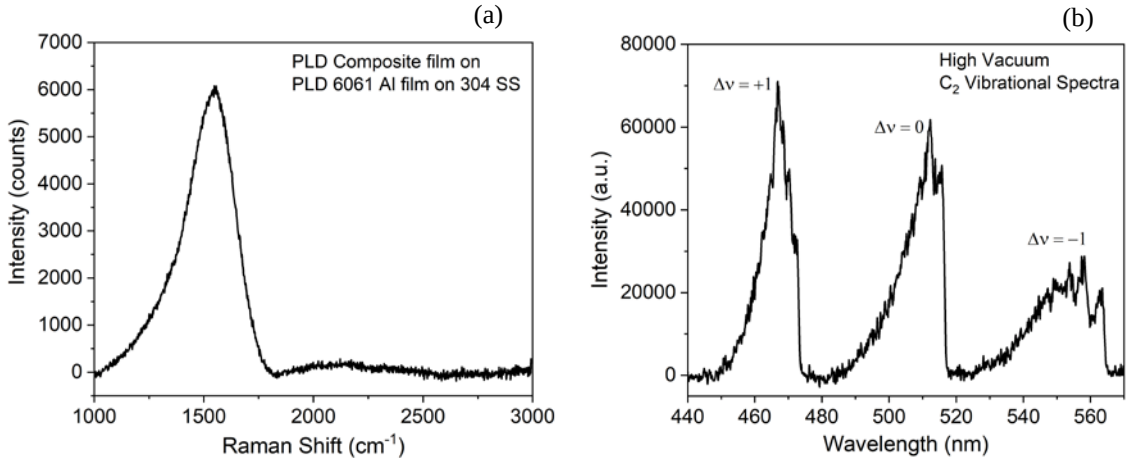

Fig. 11 Raman spectrum of PLD composite film on PLD Al-6061 film on SS 304 substrate (a); low-resolution vibrational spectra of C_2 from plume of laser ablated composite target (b)

To avoid adhesion problems of the composite on Si, a roughened Al was used as a substrate. This was followed by using a previously deposited PLD 6061 Al film on 304 SS as the substrate. Fig. 12 shows the darkening of these Al substrates upon ablation of carbon from the composite target. A visually observable darkening of both the rough Al substrate (Figs. 12 a, b) and the highly reflective PLD 6061 Al film deposited on the SS 304 (Figs. 12 c,d) can be seen.

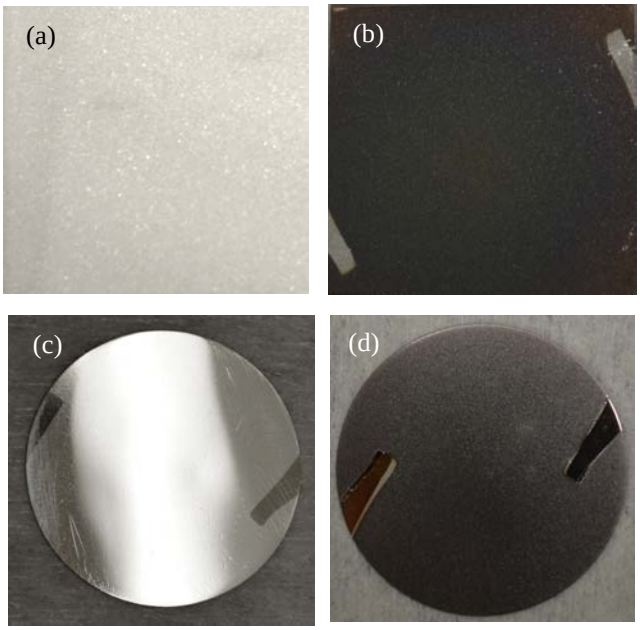

Fig. 12 Optical images of roughened Al substrate (a); PLD composite film on roughened Al substrate (b); PLD Al-6061 film on 304 SS substrate (c); PLD composite film on PLD Al-6061 film on 304 SS substrate (d)

Fig. 13 shows SEM images of the surface of the as-deposited PLD Al-6061 film (198 nm Al film thickness) and following the deposition of ablated carbon film (410 nm thick) from the composite target. Although the composite film on the 6061 Al did not crack and disintegrate like on the Si substrate, buckling of the film was observed, as can be seen in Fig. 13b.

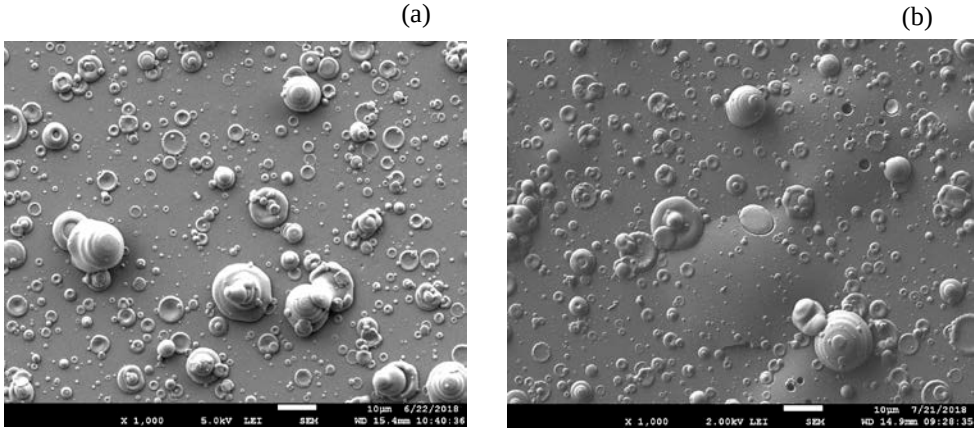

Fig. 13 SEM images of PLD Al-6061 film on 304 SS (a) and PLD Composite film on PLD Al-6061 on 304 SS (b)

Optical measurements were made on the PLD composite film (Fig. 14 a, b). Both the total and diffuse reflectance show a significant decrease from initially deposited surface of the highly reflective PLD Al 6061 film as well as the 304 SS substrate.

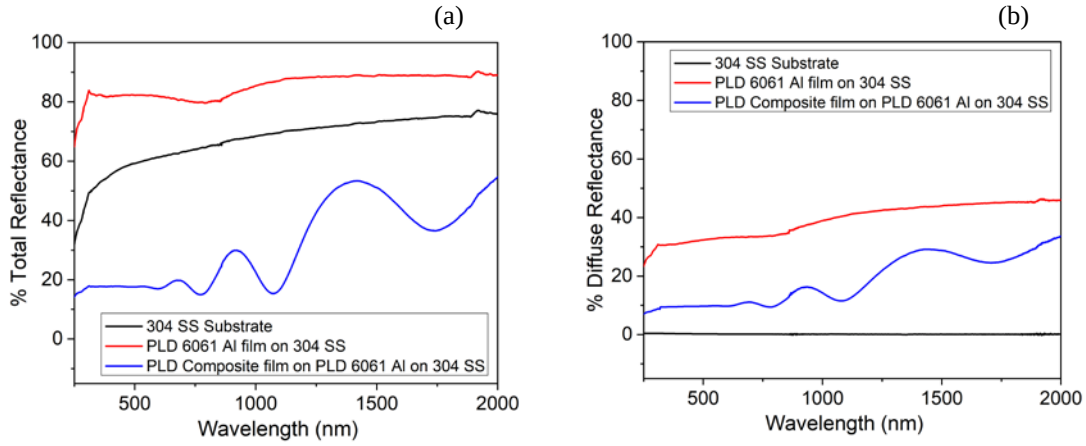

Fig. 14 Total reflectance (a) and diffuse reflectance (b) of 304 SS substrate, PLD Al 6061 film on 304 SS , and PLD composite film on 6061 Al

3. CONCLUSIONS

Our results clearly show that the primary cause of changes - either an increase or decrease - in total reflectance, is the change in the material deposited from impacts in high-vacuum (as in LEO). An additional factor affecting the reflectance values is the scattering from particles on surface. Ablation of metals, such as 6061 Al and 316 SS in 10^{-7} - 10^{-8} Torr vacuum leads to the deposition of reflective surfaces which may increase albedo. In contrast, in the presence of 2 Torr of air, filamentous Al_xO_y generated from impact to a metallic 6061 Al target is transparent, hence does not significantly alter the measured reflectance of the underlying substrate. The deposition of carbon from ablation of a composite target, over highly reflective metallic Al, causes darkening of the Al, as observed visually, and supported by a significant decrease in optical reflectance of the Al surface. This offers at least one mechanism for 'hypervelocity impact debris darkening' and is relevant to albedo interpretations leading to physical size measurement.

The albedo of hypervelocity impact fragments potentially could be increased or decreased depending on the material-dependent initial reflectance and the reflectance of the deposited impact debris, with metals producing brighter surfaces compared with carbonaceous deposits having darker surfaces. While an average albedo is used in calculating the size of orbital debris, there is a very wide range in observed albedo [6, 22]. Without knowledge of the initial albedo of an orbital debris object it would be very difficult to attribute its origin to a hypervelocity impact. This is further complicated by the phenomenon of "space weathering", where the albedo of an orbital object may change with time [22]. Our results provide an experimental determination of optical reflectance changes on pre-characterized substrates due to deposits from the laser ablation of different spacecraft materials in high vacuum.

4. REFERENCES

1. D. Hampf, P. Wagner, W. Riede, Optical Technologies for Observation of Low Earth Orbit Objects, 65th Int. Astronautical Congress, Toronto, Canada, IAC-14 A6 P, 1-8, 2014.
2. J.R. Shell, Optimizing Orbital Debris Monitoring with Optical Telescopes, AMOS 2002.
3. D. Hampf, W. Riede, G. Stockle, I. Buske, Ground-Based Optical Position Measurements of Space Debris in Low-Earth Orbits, Deutscher Luft- und Raumfahrtkongress, 301313 1-10, 2013.
4. M. Mulrooney and M. Matney, Derivation and Application of a Global Albedo Yielding an Optical Brightness to Physical Size Transformation Free of Systematic Errors, Proc. 2007 AMOS Conference, HI, 709-728, 2007.

5. M. Mulrooney, M. Matney, and E. Barker, A New Bond Albedo for Performing Orbital Debris Brightness to Size Transformations, 2008 Int. Astronautical Congress, Glasgow, Scotland.

6. A.E. Potter, K.G. Henize, and D.L. Talent in *Orbital Debris from Upper-stage Breakup*, Ed. J.P. Loftus, A90-18004 05-12, Washington, DC, AIAA 147-156, 1989.

7. H. Cowardin, K. Abernathy, E. Barker, P. Seitzer, M. Mulrooney, T. Schildknecht, An Assessment of GEO Orbital Debris Photometric Properties Derived from Laboratory-Based Measurements, *https://ntrs.nasa.gov/archive/nasa/casi.ntrs.nasa.gov/2009.*

8. Syuzo Isobe et al., A new 1 m telescope for space debris survey observations, Advances in Space Research, 34, 917 920, 2004.

9. K. Jorgensen, J. Africao, K. Hamada, E. Stansbury, P. Sydney, P. Kervin, Physical Properties of Orbital Debris from Spectroscopic Measurements, Advances in Space Research 34, 1021-1025, 2004.

10. D.J. Kessler, K.S. Jarvis, Obtaining the Propertly Weighted Average Albedo of Orbital Debris from Optical and Radar Data, Advances in Space Research 34, 1006-1012 2004.

11. A. N. Pirri, Theory for Laser Simulation of Hypervelocity Impact, Physics of Fluids, 20 221-228, 1977.

12. G. Radhakrishnan, Time-resolved spectroscopy of plasma flash from hypervelocity impact on DebriSat, The 13th Hypervelocity Impact Symposium, Procedia Eng. 103 507-514, 2015.

13. P.M. Adams, P. Sheaffer, Z. Langley, G. Radhakrishnan, Characterization of Hypervelocity Impact Debris from the DebriSat Tests, AMOS 2017 Conference, Maui, HI.

14. G. Radhakrishnan, P.M. Adams, C.J. Panetta, and D. R. Alaan, Comparison of Laser Ablation Effects to Hypervelocity Impact and Debris Darkening, paper presented at the 14th Hypervelocity Impact Symposium 2017, HVIS2017, 24-28 April 2017, Canterbury, Kent, UK, Procedia Eng. 204, 315-322 (2017).

15. G. Radhakrishnan, P.M. Adams, D. R. Alaan, C.J. Panetta, Debris Albedo from Laser Ablation in Low and High Vacuum: Comparisons to Hypervelocity Impact, AMOS 2017 Conference, Maui, HI.

16. J. T. Knudtson, W. B. Green, and D.G. Suttton, The UV-visible spectroscopy of laser-produced aluminum plasmas, J. Appl. Phys. 61 4771-4780, 1987.

17. NIST Atomic Spectra Database, http://physics.nist.gov

18. S.S. Harilal, B.E. Brumfield, B. D. Cannon, and M. C. Phillips, Shock Wave Mediated Plume Chemistry for Molecular Formation in Laser Ablation Plasmas, Anal. Chem. 88, 2296-2302, 2016.

19. R.W.B. Pearse and A.G. Gaydon, *The Identification of Molecular Spectra*, 3rd Ed., Chapman and Hall Ltd. London, 1965.

20. J. Hermann and C. Dutouqnet, Analyses of gas-phase reactions during reactive laser ablation using emission spectroscopy, J. Phys. D.: Appl. Phys. 32 2707-2714 1999.

21. A.K. Sharma and R.K. Thareja, Pulsed laser ablation of aluminum in the presence of nitrogen: Formation of aluminum nitride, J. Appl. Phys. 88 7334-7338 2000.

22. K. G. Henize, C. A., O'Neill, M. K. Mulrooney, and P. Anz-Meador, Optical properties of orbital debris, J. Spacecraft Rockets, 31, 671-677, 1994.

23. D. P. Engelhart, R. Cooper, H. Cowardin, J. Maxwell, E. Plis, D. Ferguson, D. Barton, S. Schiefer, R. Hoffmann, Space Weathering Experiments on Spacecraft Materials, AMOS 2017 Conference, Maui, HI.

24. ACKNOWLEDGEMENTS

We gratefully acknowledge Vale Sather, Sam Peresztegy, Marlon Sorge, and Tom Huynh for their support of this work. Scott Sitzman calculated film thicknesses from EDS data. Financial support was provided from AF SMC.